JOURNAL OF MATERIALS SCIENCE 32 (1997) 57–65

Preparation of $La_{1-x}Sr_xMnO_3$ powders by combustion of poly(ethylene glycol)–metal nitrate gel precursors

HYU-BUM PARK, HO-JIN KWEON*, YOUNG-SIK HONG, SI-JOONG KIM, KEON KIM
Department of Chemistry, Korea University, Sungbuk-Ku, Seoul, 136-701, Korea and
**Samsung Electronics Co., Ltd. Suwon, 442-742, Korea*

$La_{1-x}Sr_xMnO_3$ powders were prepared by auto-ignited combustion of poly(ethylene glycol) (PEG)–metal–nitrate gel precursors. The thermal behaviour of the precursors strongly depends on the ratio of PEG to metal nitrate, which is closely related to the ratio of fuel to oxidizer. The burning behaviour in a furnace was successfully explained by valence concepts normally encountered in propellant chemistry. The formation of a pure perovskite phase was significantly influenced by the homogeneity of the gel precursor. Perovskite structured oxides were formed through two different paths, one of which was direct formation from the burning of a gel precursor and the other was a subsequent structural evolution by heat treatment after burning. The formation procedure of the perovskite and the morphology of powders could be explained in terms of the burning behaviour of the precursor and the role of organic residue.

1. Introduction

The perovskite structured lanthanum-transition metal oxides substituted by alkaline earth metals are technologically important due to their electrical, magnetic and catalytic properties [1–3]. Of particular interest is strontium-substituted lanthanum manganite which has potential application as a cathode material in a solid oxide fuel cell [4]. Traditionally these materials have been prepared through a solid state route by firing mixtures of oxides or carbonates. The method requires heating of the solid reactants at high temperature for long periods of time, generally with intermittent grinding. These products frequently have compositional inhomogeneities, minor phases, and large particles.

In order to obtain homogeneous fine powders, various solution-route preparation methods have been extensively investigated. Amongst these methods, are techniques based on using organic polymers as gelling or complexing agents. In 1967, Pechini [5] invented a simple powder preparation process using polyester polymeric precursors consisting of citric acid and ethylene glycol and this process has been extensively used to produce mixed-cation oxide powders. Recently, other polymers, such as PEG(poly(ethylene glycol)) [6], PVA(poly(vinyl alcohol)) [7], PAA(poly (acrylic acid)) [8–10], and a starch-derived polymer [11], have been used to prepare metal oxides.

Manoharan and Patil [12, 14] and Suresh and Patil [13] have prepared very fine metal oxide powders using a simple and rapid *in situ* combustion process. They applied concepts [15] employed in propellant chemistry to the preparation of metal oxide powders. In this process, the elements and ions from the reactants are considered as a fuel or oxidizer and the ratio of oxidizer to fuel is controlled so as to release the maximum energy in the combustion reaction. Chakraborty *et al.* [16] have prepared $La_{1-x}Sr_xMnO_3$ powders by the auto-ignition of carboxylate–nitrate gels and Li *et al.* [6] and Saha *et al.* [7] have reported the preparation of mixed metal oxides by *in situ* auto-ignited combustion of polymeric precursors. However there is currently no detailed understanding of the burning process or the formation procedure of the metal oxide lattice from the polymeric precursor.

In this paper, we report a simple method for the preparation of homogeneous $La_{1-x}Sr_xMnO_3$ oxide powders by auto-ignited combustion. We have also investigated the formation routes of the $La_{1-x}Sr_xMnO_3$ from the PEG-metal nitrate precursors containing various ratios of PEG to metal nitrate. In order to explain the burning behaviour of the precursor and also the oxide formation route from the precursor, use is made of valence concepts that are normally applied in propellant chemistry. In addition, we have investigated the relationship between the characteristics of the synthesized powders and the burning behaviour of the precursors.

0022–2461

2. Experimental procedure

La_2O_3 (Junsei, GR), $SrCO_3$ (Junsei, EP), $Mn(NO_3)_2 \cdot xH_2O$ (Junsei, EP), and PEG (Yakuri, EP; average molecular weight = 20 000) were used as the starting materials. For manganese nitrate, a stock solution standardized using ethylenediaminetetreacetic acid (EDTA) titration was used. The preparation route of the $La_{1-x}Sr_xMnO_3$ powders is schematically illustrated in Fig. 1.

PEG–metal nitrate precursors with the compositions of $La_{1-x}Sr_xMnO_3$(x = 0.00, 0.20, 0.40 and 0.60) were prepared as follows. Initially stoichiometric amounts of La_2O_3 and $SrCO_3$ were dissolved in dilute nitric acid and then stoichiometric amounts of the manganese nitrate solution were added to the solutions. Finally PEG was added to the metal solution so that the mole ratio (R) of the PEG repeating unit to the total metal ion content was 1.25, 2.50, 5.00 and 10.0, respectively. The PEG–metal nitrate solution was heated at 60 ~ 80 °C for two days with stirring in order to evaporate excess water. As the water evaporated, the solution became viscous and the initial light-yellow colour of the solution changed to colourless. Finally, the solutions having higher R and lower x values formed clear gels.

To initiate auto-ignition, the dried precursor was placed in a furnace that had been pre heated to 300 °C. After a few minutes the precursor gel automatically ignited and burnt with the appearance of a flame. This burning process was strongly dependent on R. The burnt powders were further heated at 600, 900 and 1200 °C for 2 h in air, in order to enhance the formation of the final crystalline product and also to allow the investigation of the formation mechanism of the perovskite structured phases.

X-ray diffraction (XRD) patterns of the precursors and powders were taken with a Rigaku diffractometer

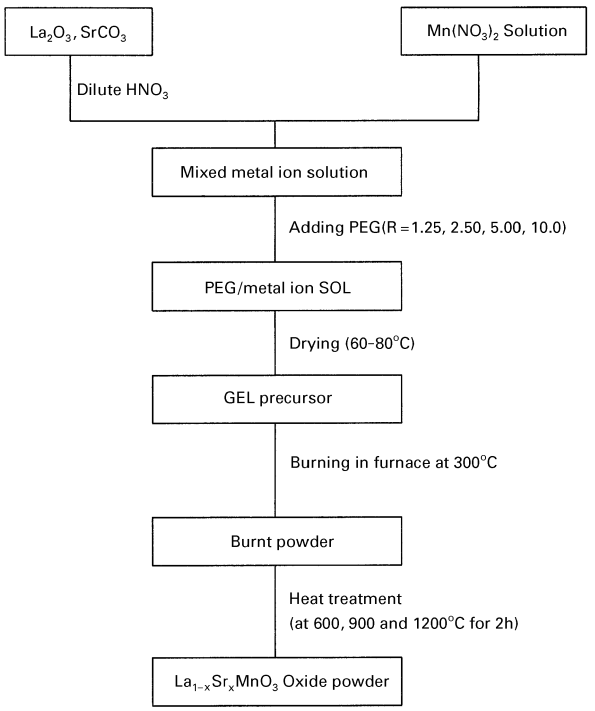

Figure 1 Flow chart for preparation of $La_{1-x}Sr_xMnO_3$ powders using PEG.

(D-MAX III) using Cu K_α radiation not only to characterize the phase of the obtained powder but to also investigate the structural evolution from the gel precursor. The crystallite size of the powder was calculated from the half-width of the diffraction peak at $2\theta = 46.7^\circ$ using the Scherrer equation [17]. Thermogravimetric analysis (TGA) and differential scanning calorimetry (DSC) were performed at a heating rate of 10 °C per min with TGA-1000 and DSC-1500 instruments from Stanton Redcroft Co. However, some precursors were explosive and thus a part of the samples were removed from the sample container. Therefore, it was difficult to obtain quantitative DSC and TG curves in the higher temperature region. Fourier transform infra-red (FT-IR) spectra of pressed pellets with KBr were measured using a Bomem(MB-102) spectrophotometer. The specific surface area was measured by the Brunauer–Emmett–Teller (BET) method using N_2 gas with a Quantachrome Autosorb. Scanning electron micrographs (SEM) were taken with a Hitachi S-4100 microscope.

3. Results and discussion

3.1. Preparation of the gel precursor

PEG was used to enhance the homogeneous mixing of the metal cations and also to suppress the crystallization of metal nitrates. Since PEG has ether oxygens in its chain, it can interact with metal ions [18]. The interaction and the random arrangement of the polymer chain possibly hinder the crystallization during evaporation of the water from the mixed solution and thus enhance mixing of metal cations on the molecular level. In order to prepare a homogeneous gel precursor, a higher ratio of PEG to metal ion might be favourable. In order to preserve charge balance, nitrate anions are required to remain in the gel precursors.

During evaporation of the mixed solution, precipitates were observed for higher Sr contents and also for lower R values (Table I). For the $LaMnO_3$ gel precursor, the solution with R = 1.25 produced a white crystalline precipitate, but solutions with other ratios did not produce a precipitate. The crystalline precipitate was identified as $Mn_3La_2(NO_3)_{12} \cdot 24H_2O$ by reference to the XRD pattern of $Mg_3La_2(NO_3)_{12} \cdot 24H_2O$ (JCPDS No. = 12-0761). When R = 5.00, white precipitates were also observed for x = 0.40 and 0.60 with the amount of precipitate for x = 0.60 being larger than for x = 0.40. XRD patterns of these precursors showed only a few very weak diffraction lines and were difficult to identify.

3.2. Burning behaviour of the precursors

When the dried precursors were placed in a furnace at 300 °C, it took a few minutes for the precursors to ignite automatically. The burning behaviour was strongly dependent on the value, R which was related to the ratio of fuel (PEG) to oxidizer (NO_3). For R = 1.25, if the precursor ignited at a part of the bulk precursor then a weak flame propagated through the bulk of the precursor, like a burning fuse, giving out an

TABLE I Compositions of $La_{1-x}Sr_xMnO_3$ that form a clear gel precursor during the evaporation of water

x	R (PEG units per metal ion)			
	1.25	2.50	5.00	10.0
0.00	precipitate $Mn_3La_2(NO_3)_{12}\cdot 24H_2O$	clear	clear	clear
0.20	precipitate	precipitate(?)	clear	clear
0.40	–	precipitate	precipitate $Sr(NO_3)_2$(?)	–
0.60	–	–	precipitate $Sr(NO_3)_2$(?)	–

clear: clear gel precursor formation, precipitate: precipitate formation.

odour of decomposing nitrate salt and the resulting powder was fluffy. For R = 2.50, the gel precursor burnt explosively with a large yellow-orange flame and the burning was completed in a few seconds. For R = 5.00, an explosive reaction occurred initially with a large orange-red flame which was followed by a small red flame with black smoke which continued for a few minutes and finally a faint dark-red light without any flames was emitted for several minutes. The product was a soft and slightly sticky lumped powder. For R = 10.0, the burning behaviour was similar to that observed for R = 5.00, however a longer time was required for it to burn out.

These results can be explained by recourse to the concepts of propellant chemistry used by Manoharan and Patil [12, 14] and Suresh and Patil [13]. They applied the valence concepts for condensed fuel–oxidizer mixtures proposed by Jain *et al.* [15] to prepare various metal oxides by combustion process and they then calculated the stoichiometric composition of fuel and oxidizer to release the maximum energy from their combustion reaction system. According to the applied concepts, the elements C, H, La, Sr and Mn are considered as reducing species with the corresponding valences, +4, +1, +3, +2 and +2, respectively. The oxygen is considered as the oxidizing species with valence −2. The valence of nitrogen is considered to be zero. When the ratio of total reducing valence to total oxidizing valence is 1.00, the energy released from combustion reaction is a maximum. In the present study the valences of the reaction species, $(-CH_2CH_2O-)$, NO_3^- and metal cations, can be calculated as +10, −6 and +3 (or +2), respectively. For $LaMnO_3$ gel precursor, when R = 1.25, 2.50, 5.00 and 10.0, the ratios of the reducing valence to oxidizing valence correspond to 1.00, 2.00, 4.00 and 8.00, respectively. Therefore it is expected that the combustion process of R = 1.25 releases the maximum heat and thus is the most violent. However, the precursor of R = 1.25 was inhomogeneous and contained precipitate of nitrate. On burning, the precipitate was decomposed by combustion heat, which resulted in the noticed odour of decomposing nitrate. Among precursor forming homogeneous gels, the precursor of R = 2.50, which had valence ratio (= 2.00) closest to 1.00, burnt most violently. On the other hand, the precursors of R = 5.00 and 10.0 have excess PEG and the occurrence of a red flame with black smoke indicates that the excess organic moiety burned after exhaustion of the oxidizer. Thus the burning behaviours of the precursors can be explained by the concepts of oxidizing and reducing valence used in propellant chemistry.

3.3. Thermal analysis

The pyrolysis of the $LaMnO_3$ gel precursor was studied by thermal analysis and compared with that of pure PEG (Figs 2 and 3). The DSC curves for PEG show two endothermic peaks at 65 and 400 °C, broad exothermic peaks between 200–340 °C, and another exothermic peak at 670 °C. These peaks are tentatively ascribed to melting, the evaporation of decomposed organic moiety, the burning of PEG, and the burning of carbonaceous residue, respectively. The gel precursors show endothermic peaks corresponding to water evaporation with weight losses at 79 °C and at 138 °C for R = 1.25, and at 156 °C for R = 2.50, and at 131 °C for R = 5.00. The precursors have exotherms showing two different patterns between 180–450 °C and the exotherms are probably caused by the combustion of PEG. Whereas the precursors of R = 1.25 and 2.50 show a very strong and sharp exotherm at about 200 °C and a subsequent exotherm at about 300 °C, the precursor of R = 5.00 shows large and broad exotherms in the whole exotherm region. TG curves of the precursors show drastic weight losses at lower

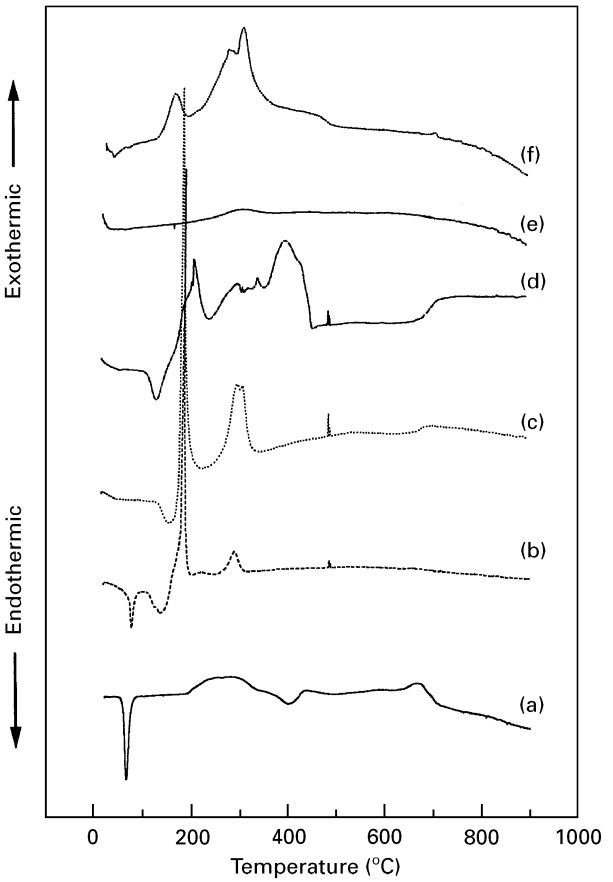

Figure 2 DSC curves for (a) pure PEG and for $LaMnO_3$ gel precursors with R values of (b) 1.25, (c) 2.50, and (d) 5.00 and also for powders after burning with R values of (e) 2.50 and (f) 5.00.

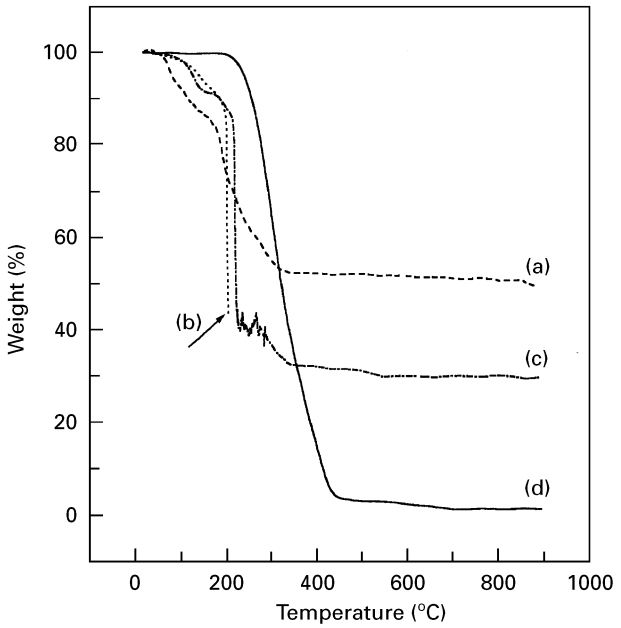

Figure 3 TG curves for $LaMnO_3$ gel precursors with R values of (a) 1.25, (b) 2.50 and (c) 5.00 and also for (d) pure PEG.

temperature than pure PEG. If we compare the temperatures of initial exotherm and weight loss of the precursors with those of pure PEG, it seems that a catalytic combustion occurs by the metal nitrate in the gel precursors. This is especially true, for R = 1.25 and 2.50, where a very sharp and strong exothermic peak appears at 200 °C. The resulting heat can raise the temperature of the combustion system and cause crystallization and sintering. For R = 5.00, the large exotherm above 350 °C may be due to the combustion of excess PEG.

DSC curves of the burnt powders at about 300 °C show large exotherms for R = 5.00 but only a small exotherm for R = 2.50. This indicates that the burnt powder still has a large amount of organic residue for R = 5.00, but only a small amount for R = 2.50.

3.4. Structural analysis by XRD and IR

XRD patterns of the powders were measured in order to investigate the influence of Sr content on the formation of $La_{1-x}Sr_xMnO_3$ oxides from a gel precursor with R = 5.00. The XRD patterns of calcined powders at 600 °C for 2 h are illustrated in Fig. 4. For higher Sr contents (x = 0.40, 0.60), $SrCO_3$ is formed in addition to the cubic perovskite phase, but for lower Sr contents only the cubic phase is obtained. When lanthanum manganates and cobaltates containing higher Sr contents were prepared at low temperatures, $SrCO_3$ was frequently observed due to the stability of the carbonate form of Sr [9, 16, 19–21]. During the preparation of the precursor, a precipitate was formed for higher Sr content compositions (x = 0.40 and 0.60). Considering the solubility of the nitrate salts and the observed weak diffraction lines of the gel precursors containing a higher Sr content, the precipitate is thought to be $Sr(NO_3)_2$. In the burning process, the evolved CO_2 gas can react with Sr^{2+} ions and produce $SrCO_3$. IR spectra of these samples showed peaks that could be assigned to carbonate ions. However, the samples were transformed into a pure perovskite phase by a further heat treament at a higher temperature (900 or 1200 °C).

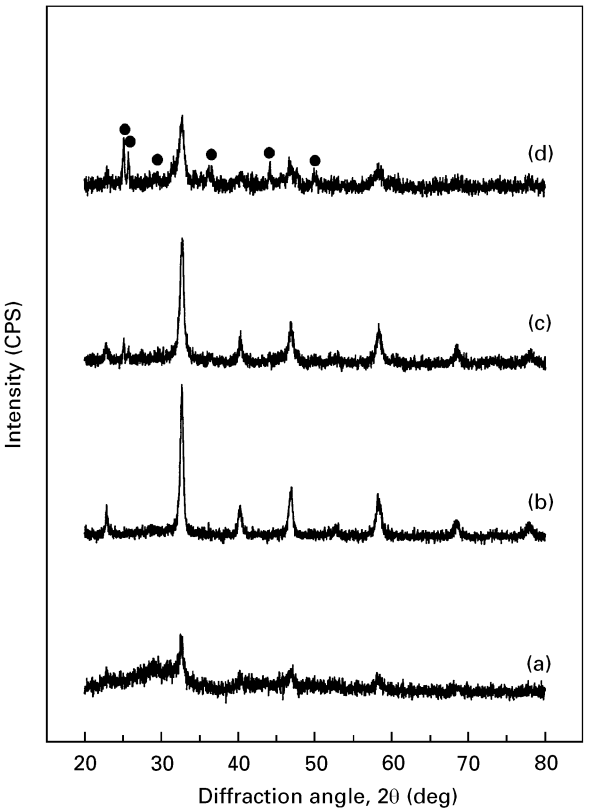

Figure 4 XRD patterns of $La_{1-x}Sr_xMnO_3$ powders with R = 5.00 obtained by a heat treatment at 600 °C for 2 h. The values of x investigated are (a) 0.00, (b) 0.20, (c) 0.40 and (d) 0.60. The presence of $SrCO_3$ as an impurity phase is denoted by (●).

XRD patterns of $LaMnO_3$ calcined at 600 °C for 2 h are shown in Fig. 5. The patterns show sharp diffraction peaks that can be indexed in terms of a single phase rhombohedral perovskite for R = 1.25 and 2.50 whilst only broad weak lines of a pseudocubic perovskite are observed for R = 5.00 and 10.0. IR spectra of $LaMnO_3$ calcined at 600 °C for 2 h were recorded and are shown in Fig. 6. It is well known that $LaMnO_3$ shows two strong bands at 610 cm^{-1} for M–O stretching and at 390 cm^{-1} for O–M–O bending [22, 23]. IR spectra for lower R values show two separated bands at 610 cm^{-1} and 390 cm^{-1} which is indicative of the complete formation of the crystal lattice. However, for higher R values the two bands are partially separated and two additional bands are observed around 1480 cm^{-1} and 1390 cm^{-1}. The additional bands at higher frequency are presumed to be caused by metal carbonate [24, 25].

The formation area of pure perovskite and the crystal structure of perovskite formed by heat treatment at 600 °C for 2 h are summarized in Table II. For the samples with higher R values and lower x, pure perovskite structured phases were easily formed and the formation area of pure perovskite agrees with that of homogeneous gel precursors (Table I) with the exception of $LaMnO_3$ of the sample with R = 1.25. Therefore, to achieve a pure perovskite phase it is necessary to prepare a homogeneous gel precursor. DSC curves of the precursors having lower R values showed a very

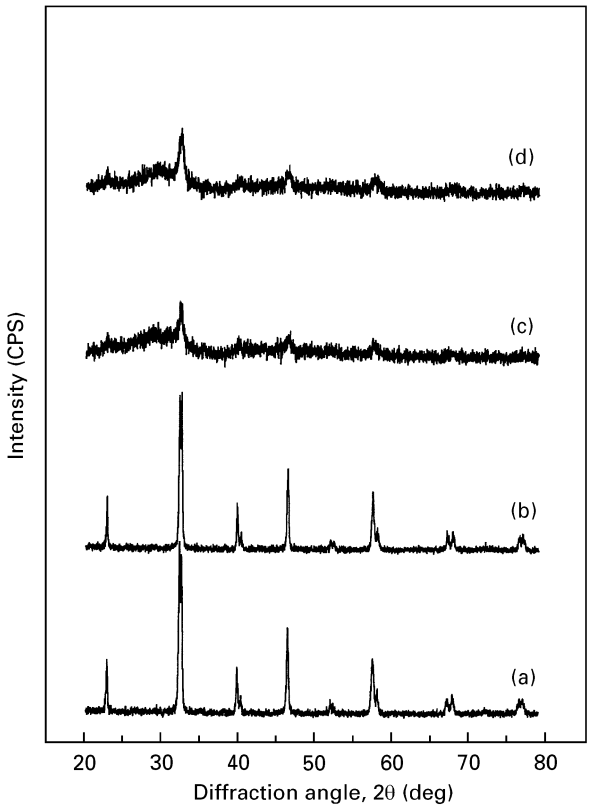

Figure 5 XRD patterns of $LaMnO_3$ powders with R values of (a) 1.25, (b) 2.50, (c) 5.00 and (d) 10.0, obtained by a heat treatment at 600 °C for 2 h.

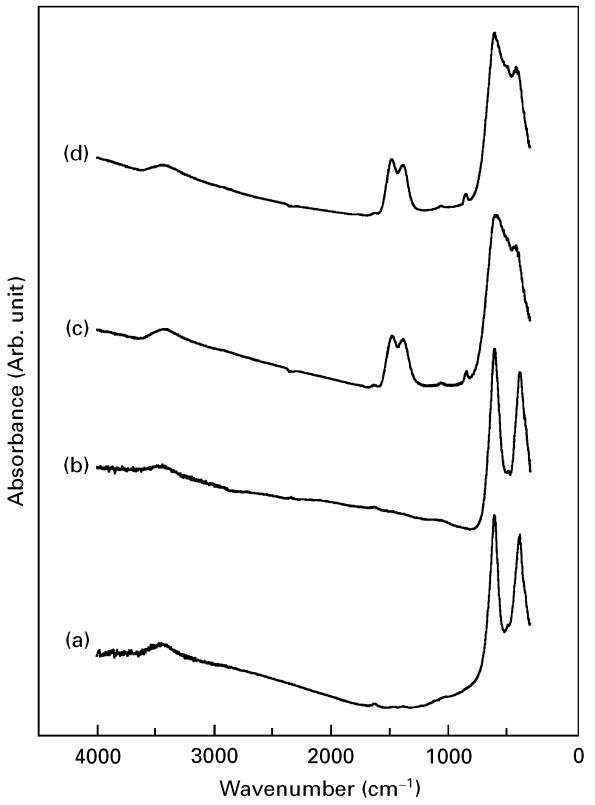

Figure 6 IR spectra of $LaMnO_3$ powders with R values of (a) 1.25, (b) 2.50, (c) 5.00 and (d) 10.0, obtained by a heat treatment at 600 °C for 2 h.

sharp and strong exotherm at about 200 °C. This heat can promote the formation of the perovskite phase. However for higher R value samples, the precursors are in a fuel rich condition and the combustion heat released at the burning stage is relatively small, and futhermore the combustion heat is partially consumed in order to raise the temperature of the excess fuel. In this case, a metastable pseudocubic phase is formed with an impurity amorphous carbonate phase the presence of which is inferred from the IR spectra.

TABLE II Phases obtained after a heat treatment of 600 °C for 2 h

x	R (PEG units per metal ion)			
	1.25	2.50	5.00	10.0
0.00	rhombohedral	rhombohedral	cubic (weak)	cubic (weak)
0.20	rhombohedral (+impurity)	rhombohedral (+impurity)	cubic	cubic
0.40	–	–	cubic (+$SrCO_3$)	–
0.60	–	–	cubic (+$SrCO_3$)	–

(weak): weak diffraction lines,
(+impurity): additional diffraction line of unknown impurity phase,
(+$SrCO_3$): additional diffraction lines of $SrCO_3$.

3.5. The perovskite formation process

On the whole, we could find two formation paths of crystalline perovskite, which significantly depended on R. For R = 2.50 (Fig. 7), well-crystallized orthorhombic perovskite forms directly from the amorphous precursor only by auto-ignited burning at 300 °C and it subsequently changes to a rhombohedral symmetry by heat treatment at 600 °C. When R = 1.25, the same structural development was observed. Taguchi *et al.* [26] reported a similar consecutive change of structure in the preparation of $LaMnO_3$ using PAA. In addition Manoharan and Patil [14] reported that the orthorhombic phase of $LaMnO_3$ could be directly prepared by a one step combustion route. Using auto-ignited combustion, we could prepare perovskite structured powders at low temperatures, for example 300 °C at low R values. However, for R = 5.00 (Fig. 8), the burnt powder is still amorphous and further heat treatment produces a pseudo-cubic perovskite and finally a rhombohedral structured phase is established. The intermediate cubic phase often appears in the preparation of lanthanum manganate using organic precursors [9, 11, 16].

IR spectra (Figs 9 and 10) obtained from successive heat treatments support the XRD results and confirm the existence of two different paths of structure development. The precursors show many peaks, such as an O–H stretching band of water at 3450 cm^{-1}, a C–H stretching band at 2920 cm^{-1} and many complex bands corresponding to the stretching and bending of PEG and NO_3^- below 1700 cm^{-1}. Although the burnt powder with R = 2.50 (Fig. 9) shows nearly separated bands the correspond to the stretching and bending of M–O bonds at 590 cm^{-1} and 385 cm^{-1}, the sample with R = 5.00 (Fig. 10) contains broad bands that appear in the region corresponding to M–O bonds but also many bands corresponding to organic residuals

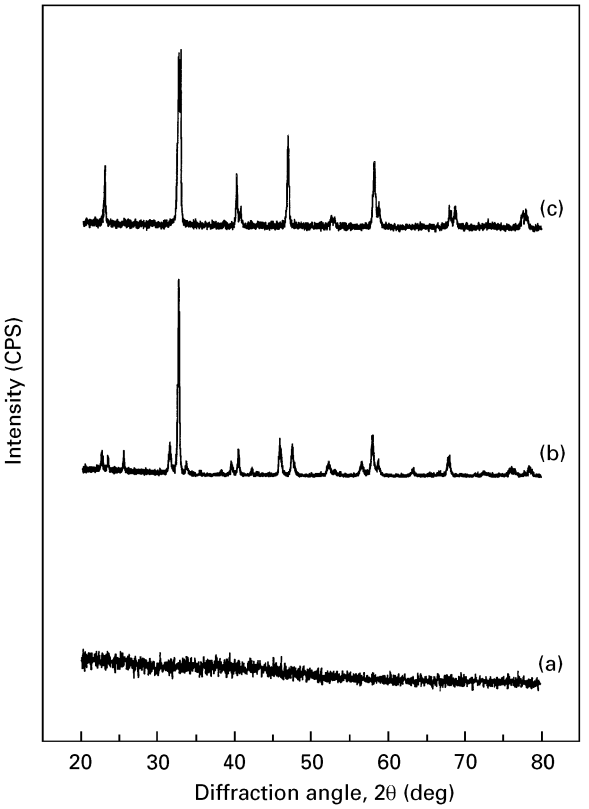

Figure 7 XRD patterns of $LaMnO_3$ powders with R = 2.50 obtained by consecutive heat treatments of the gel precursor. The thermal histories considered are (a) gel precursor, (b) powder after burning and (c) 600 °C 2 h.

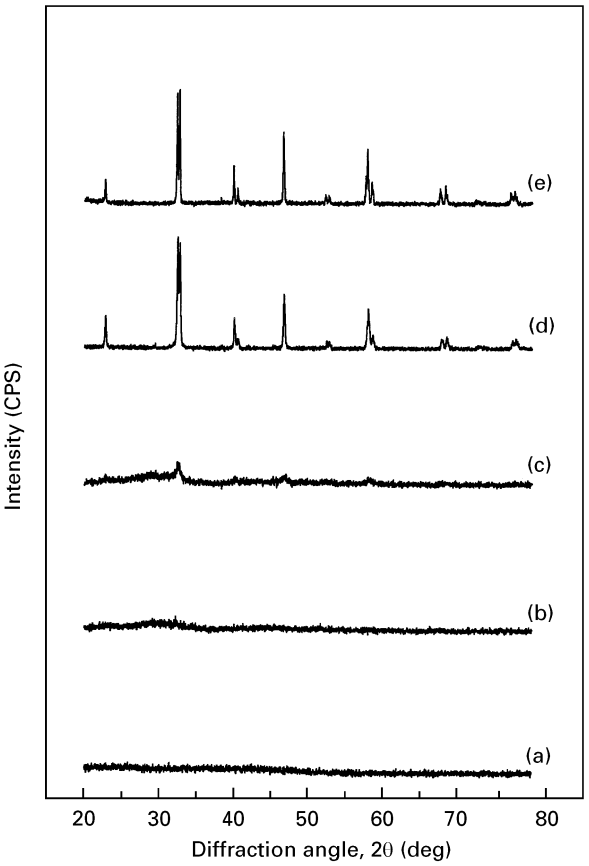

Figure 8 XRD patterns of $LaMnO_3$ powders with R = 5.00 obtained by consecutive heat treatments of the gel precursor. The thermal histories considered are (a) gel precursor, (b) powder after burning, (c) 600 °C 2 h, (d) 900 °C 2 h and (e) 1200 °C 2 h.

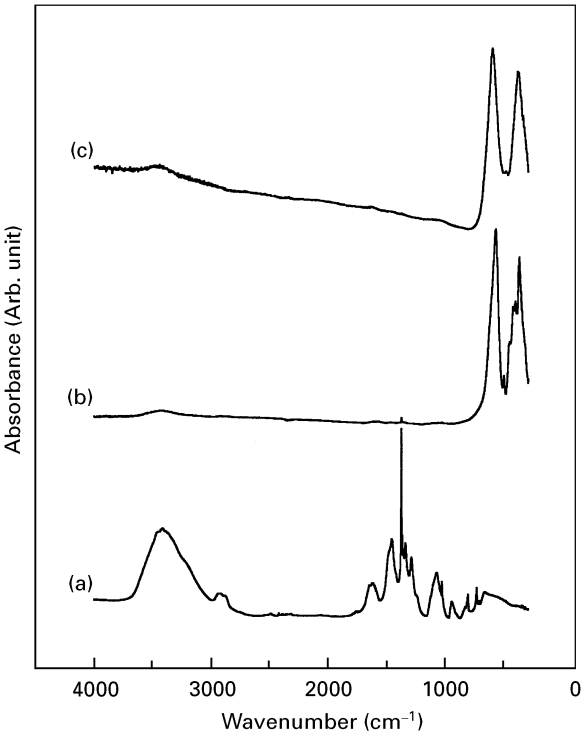

Figure 9 IR spectra of $LaMnO_3$ powders with R = 2.50 obtained by consecutive heat treatments of the gel precursor. The thermal histories considered are (a) gel precursor, (b) powder after burning and (c) 600 °C 2 h.

and NO_3^- still remain. A subsequent heat treatment at 600 °C enhances the intensity and the separation of the M–O bands and produces doublet bands around 1430 cm^{-1}, thought to be due to bands associated with amorphous carbonate. After a further heat treatment at 900 °C, clear M–O bands are evident and the higher energy bands disappear (the band observed at 3450 cm^{-1} is due to water absorbed by KBr).

As previously reported in the literature [26–28], the crystal symmetry of lanthanum manganate is largely infuenced by the oxygen stoichiometry, which is a function of the concentration of Mn^{4+} ions. Takeda *et al.* [28] have reported a relationship between the crystal symmetry and the oxygen content for quenched $(La_{1-x}A_x)_{1-y}MnO_{3+z}$ after annealing at various temperature. Kamata *et al.* [29] have reported that the oxygen content of $LaMnO_{3+2}$ depended on the partial pressure of oxygen during annealing. Also, according to the data of the Joint Committee on Powder Diffraction Standards, $LaMnO_{3.00}$ (No. = 35–1353) is orthorhombic whilst $LaMnO_{3.15}$ (No. = 32–484) has a rhombohedral symmetry. When the oxygen content is near 3.00, the crystal symmetry of manganate is orthorhombic. For oxygen contents of 3.12–3.17, the crystal symmetry is rhombohedral. The crystal structure of $LaMnO_{3+z}$ changes from orthorhombic to rhombohedral symmetry when 3+z is about 3.05.

Taguchi *et al.* [26] suggested that the orthorhombic phase was produced under low oxygen partial pressures during the preparation of $LaMnO_3$. For R = 2.50, the burning process was completed in a very short time with the release of a large amount of heat and thus it might produce products having reducing

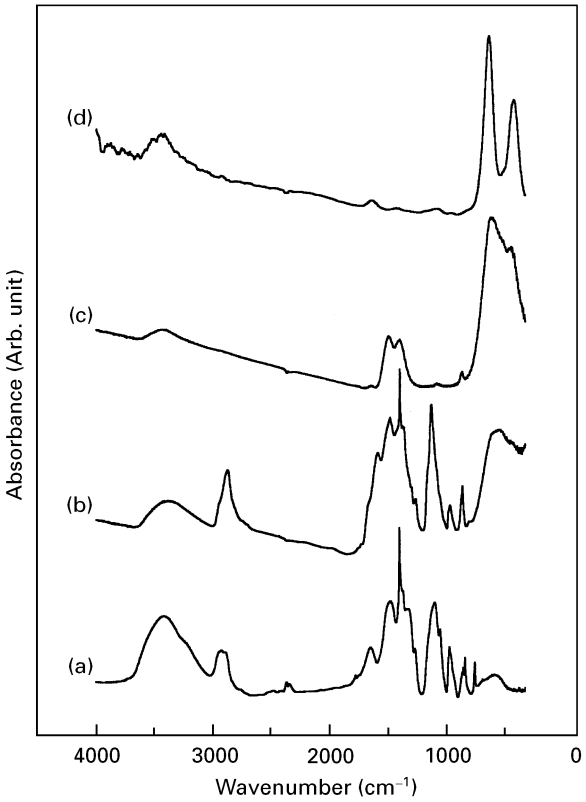

Figure 10 IR spectra of $LaMnO_3$ powders with R = 5.00 obtained by consecutive heat treatments of the gel precursor. The thermal histories considered are (a) gel precursor, (b) powder after burning, (c) 600 °C 2 h and (d) 900 °C 2 h.

power, such as CO gas, by incomplete combustion. The resultant low oxygen partial pressure could suppress the oxidation of Mn^{2+} to Mn^{4+}. Consequently, the orthorhombic phase which has a lower oxygen content is produced. If oxygen is supplied from air in sufficient quantities during annealing at 600 °C, then the orthorhombic phase changes to the more stable rhombohedral form. On the other hand, it can be suggested from the IR and XRD results that the perovskite structure is completely formed above 900 °C via a metastable pseudocubic phase for samples with R = 5.00. In this case, the excess PEG is not completely oxidized by the nitrate at the burning stage and residual organic materials remain to high temperature. It is possible that these residues hinder the formation of the perovskite structured material before complete burning out. Therefore, the structure gradually develops as the temperature of the heat treatment is increased.

3.6. Characterization of powders

Representative SEM photographs of the powders are shown in Figs 11(a and b) and 12(a and b). The microstructure of a $LaMnO_3$ powder prepared from a precursor with R = 2.50 shows large hardened agglomerates containing pores presumably caused by violent gas evolution (Fig. 11(a)) and with a shape similar to a sintered ceramic body (Fig. 11(b)). This

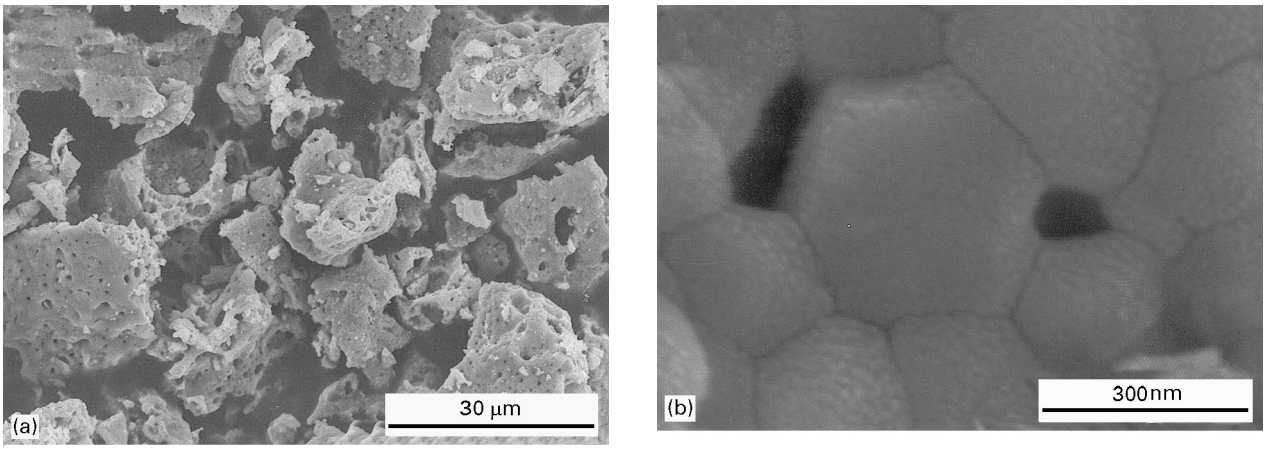

Figure 11 SEM photographs for $LaMnO_3$ powders with R = 2.50 obtained by heat treatment at 600 °C for 2 h.

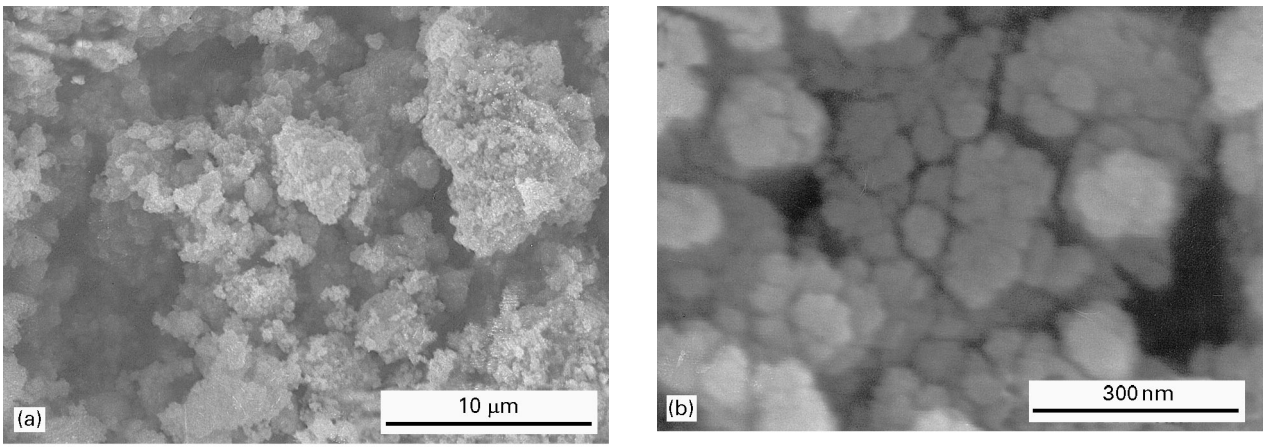

Figure 12 SEM photographs for $LaMnO_3$ powders with R = 5.00 obtained by heat treatment at 600 °C for 2 h.

TABLE III BET surface areas and crystallite sizes of $LaMnO_3$ powders formed by subsequent heat treatment after furnace burning

R	Heat treatment	Surface area ($m^2 g^{-1}$)	Crystallite size (nm)
1.25	–	2.99	–
2.50	–	1.62	–
5.00	–	0.97	–
1.25	600 °C 2 h	3.45	120
2.50	600 °C 2 h	1.92	150
5.00	600 °C 2 h	7.09	24

feature supports the idea that partial sintering of particles occurred due to the combustion heat. However the SEM photographs obtained on a sample from a precursor with R = 5.00 show soft agglomerated lumps (Fig. 12(a)) with a clear shape of fine particles (Fig. 12(b)). The individual particles are very fine with a size of several tens of nanometers, however they are also considerably agglomerated.

The BET surface area and crystallite sizes calculated using the Scherrer equation [17] are listed in Table III. The surface areas of powders calcined at 600 °C are larger than powders burnt in the furnace, especially, for R = 5.00. This is indirect evidence for the existence of organic materials after the burning stage. The organic residue fills the spaces between particles formed by burning and thus reduces the surface area. The surface area of $LaMnO_3$ decreases in value from R = 1.25 to 2.50 and reaches its maximum value for R = 5.00. The crystallite size shows a reverse tendency. When the ratio of PEG to metal ion is high, powders having large surface areas are formed. Thus an excess of PEG is important in order to obtain fine powders and enhance the surface area.

4. Conclusions

$La_{1-x}Sr_xMnO_3$ powders were prepared via the auto-ignited combustion of PEG–metal nitrate gel precursors. A pure perovskite structured phase was easily formed from clear homogeneous precursors having a high PEG content and a low Sr content. As expected from the application of valence concepts used in propellant chemistry, the thermal behaviour is sensitive to the ratio of PEG to metal nitrate. The combustion of a precursor with a small PEG content instantaneously releases large amounts of heat and produces partially sintered powders with a small surface area and large crystallite size. However, a precursor containing an excess of PEG does not show any sharp exotherms, and an organic residue from the PEG may prevent sintering of the fine particles formed by combustion and consequently powders having a large surface area are produced. The morphology and the surface area are greatly influenced by the ratio of PEG to metal nitrate which is also explained by the combustion heat and the residual organic material.

There are two routes to perovskite structured material formation which are distinguished by R. For lower R values, highly crystallized orthorhombic perovskites are directly prepared from the burning of precursors at 300 °C and the orthorhombic phase can be subsequently transformed into the rhombohedral phase. For higher R values, the rhombohedral perovskite is gradually built up from amorphous burnt powders by successive heat treatments, that reduce the amount of organic residue. The two routes can be understood in terms of the thermal behaviour of the precursors and the role of the organic residue. It was possible to prepare $LaMnO_3$ powder at 300 °C for lower R values.

In conclusion, $La_{1-x}Sr_xMnO_3$ powders have been successfully prepared via an auto-ignited combustion reaction and the formation procedure and the morphology of the powders can be elucidated by reference to the thermal behaviour of precursors and the role of organic residue.

Acknowledgements

This work was financially supported by the Korea Science & Engineering Foundation.

References

1. T. HASHIMOTO, N. ISHIZAWA, N. MIZUTANI and M. KATO, *J. Mater. Sci.* **23** (1988) 1102.
2. J. B. GOODENOUGH, *Phys. Rev.* **100** (1955) 564.
3. T. ARAKAWA, A. YOSHIDA and J. SHIOKAWA, *Mater. Res. Bull.* **15** (1980) 269.
4. N. Q. MINH, *J. Amer. Ceram. Soc.* **76** (1993) 563.
5. M. P. PECHINI, US Patent No. 3330 697, July (1967).
6. X. LI, H. ZHANG, F. CHI, S. LI, B. XU and M. ZHAO, *Mater. Sci. Eng. B* **18** (1993) 209.
7. S. K. SAHA, A. PATHAK and P. PRAMANIK, *J. Mater. Sci. Lett.* **14** (1995) 35.
8. P. A. LESSING, *Amer. Ceram. Soc. Bull.* **68** (1989) 1002.
9. H. TAGUCHI, D. MATSUDA and M. NAGAO, *J. Amer. Ceram. Soc.* **75** (1992) 201.
10. H. TAGUCHI, D. MATSUDA, M. NAGAO, and H. SHIBAHARA, *J. Mater. Sci. Lett.* **12** (1993) 891.
11. L.-W. TAI, H. U. ANDERSON and P. A. LESSING, *J. Amer. Ceram. Soc.* **75** (1992) 3490.
12. S. S. MANOHARAN and K. C. PATIL, *ibid* **75** (1992) 1012.
13. K. SURESH and K. C. PATIL, *J. Solid State Chem.* **99** (1992) 12.
14. S. S. MANOHARAN and K. C. PATIL, *J. ibid* **102** (1993) 267.
15. S. R. JAIN, K. C. ADIGA and V. R. P. VERNEKER, *Combustion and Flame* **40** (1981) 71.
16. A. CHAKRABORTY, P. S. DEVI and H. S. MAITI, *Mater. Lett.* **20** (1994) 63.
17. B. D. CULLITY "Elements of X-ray Diffraction" (Addison–Wesley, Seoul, 1978).
18. T. OKADA, *Analyst* **118** (1993) 959.
19. H.-M. ZHANG, Y. TERAOKA and N. YAMAZOE, *Chem. Lett.* (1987) 665.
20. Y. TERAOKA, H. KAKEBAYASHI, I. MORIGUCHI and S. KAGAWA, *Chem. Lett.* (1991) 673.
21. M. S. G. BAYTHOUN and F. R. SALE, *J. Mater. Sci.* **17** (1982) 2757.
22. G. V. S. RAO, C. N. R. RAO and J. R. FERRARO, *Appl. Spectroscopy* **24** (1970) 436.
23. Y. WU, Z. YU and S. LIU, *J. Solid State Chem.* **112** (1994) 157.

24. C. E. WEIR and E. R. LIPPINCOTT, *J. Research of the National Bureau of Standards A* **65A** (1961) 173.
25. R. P. TURCOTTE, J. O. SAWYER and L. EYRING, *Inorg. Chem.* **8** (1969) 238.
26. H. TAGUCHI, H. YOSHIOKA, D. MATSUDA and M. NAKAO, *J. Solid State Chem.* **104** (1993) 460.
27. A. WOLD and R. J. ARNOTT, *J. Phys. Chem. Solids* **9** (1959) 176.
28. Y. TAKEDA, S. NAKAI, T. KOJIMA, R. KANNO, N. IMANISHI, G. Q. SHEN, O. YAMAMOTO, M. MORI, C. ASAKAWA and T. ABE, *Mater. Res. Bull.* **26** (1991) 153.
29. K. KAMATA, T. NAKAJIMA and T. HAYASHI, *ibid* **13** (1978) 49.

Received 14 August 1995
and accepted 13 June 1996